JOURNAL OF SOLID STATE CHEMISTRY 109, 197–202 (1994)

Crystal Structure Refinements of Zircon-Type MVO_4 (M = Sc, Y, Ce, Pr, Nd, Tb, Ho, Er, Tm, Yb, Lu)

Bryan C. Chakoumakos, Marvin M. Abraham, and Lynn A. Boatner

Solid State Division, Oak Ridge National Laboratory, Oak Ridge, Tennessee 37831-6056

Received May 13, 1993; accepted July 14, 1993

Improved structural parameters for the lanthanide orthovanadates (including also YVO_4 and $ScVO_4$ and new results for $PrVO_4$, $TmVO_4$, and the $LuVO_4$ end members) have been determined by employing a full-profile Rietveld structure analysis of neutron powder-diffraction data. High-quality powders of the zircon-type MVO_4 vanadates were prepared by a homogeneous coprecipitation in molten urea. The zircon structure has space group symmetry $I4_1/amd$, $Z = 4$, with 3 atoms occupying the asymmetric unit. In all, 22 parameters were refined with final agreement values of R_p = 0.0313–0.0421, R_{wp} = 0.0361–0.0511, and G-of-F = 1.210–1.962. The average V–O bond length for all of the MVO_4 samples is 1.709(2) Å, and the V–O distance exhibits a small systematic shortening with decreasing M atom size. The oxygen positional parameters, the cell dimensions, and the M–O distances vary systematically with the metal-ion atomic number. The anisotropic thermal motion of the oxygen atom has the largest amplitude normal to the shared polyhedral edge between the VO_4 tetrahedron and MO_8 bisdisphenoid. Empirical relations are given for the cell dimensions and oxygen atom position as a function of the size of the lanthanide ion which can be used to estimate structural parameters for other zircon-type lanthanide vanadate end-members and vanadate solid solutions.

INTRODUCTION

Lanthanide and related orthovanadate compounds are of interest due to their unusual magnetic characteristics and useful luminescent properties. These materials have been employed as model systems for the investigation of polymorphism among the ABO_4-type compounds since the zircon-type vanadates have been found to transform reconstructively to the denser scheelite structure at pressures of a few kilobars and temperatures less than 600°C. High-precision crystal-structure refinements of the zircon-type vanadates have been previously reported only for $CeVO_4$ (1) and $NdVO_4$ (2), both investigations employing single-crystal X-ray diffraction data. In addition, low-precision structural refinements have been reported for the $LnVO_4$ (Ln = Tb, Dy, Er, Ho, Yb) members (3–5) using neutron powder diffraction data, which were primarily collected at low temperature and were not refined by means of the Rietveld method (e.g., using full-pattern fitting). In the present study, we have used a straightforward synthesis technique to produce high-quality powders of the subject vanadate compounds MVO_4, (M = Sc, Y, Ce, Pr, Nd, Tb, Ho, Er, Tm, Yb, Lu), and have performed structural refinements (including new refinements for Pr, Tm, and the Lu end-member) by employing Rietveld structure analysis of neutron powder diffraction data.

EXPERIMENTAL

High-quality powders of the zircon-type MVO_4 vanadate compounds were prepared by means of homogeneous coprecipitation in molten urea (6, 7). Stoichiometric amounts of the M_2O_3 oxide and ammonium vanadate (NH_4VO_3) were dissolved in a 6 N HNO_3 solution. After the addition of urea and a gradual heating (to 400°C) in order to evaporate the liquid, a final calcination at 1000°C removed all traces of the urea and yielded a fine powder of the desired vanadate. By varying the quantity of urea added, the mean particle size could be reduced (6). The phase purity of the samples was verified by X-ray powder diffraction. Several attempts to synthesize zircon-type $LaVO_4$ failed. In spite of repeated accurate duplications of alternative and supposedly proven synthesis methods (8, 9), only the monazite structural-type $LaVO_4$ was obtained. Except for $LaVO_4$ and $PmVO_4$, all of the zircon-type lanthanide vanadates were synthesized; however, neutron powder-diffraction data were not collected for $SmVO_4$, $EuVO_4$, $GdVO_4$, and $DyVO_4$ because of their high neutron-absorption cross sections.

Neutron-diffraction data were collected using the HB4 high-resolution powder diffractometer at the High-Flux Isotope Reactor at ORNL. This instrument has a Ge (115) monochromator which, when $2\theta = 80°$, selects an incident neutron beam of $\lambda \approx 1.4$ Å. The neutron wavelength was determined more precisely to be 1.416 Å on the basis of unit cell refinements for a nickel powder standard. Soller slit collimators of 12′ and 20′ are positioned before and

0022-4596/94 $6.00

after the monochromator crystal, respectively. An array of 32 equally spaced (2.7°) ^{3}He detectors, each with a 6′ mylar foil collimator, can be step-scanned over a range of up to 40° for scattering angles between 11° and 135°. The samples were placed in vanadium cans (9 mm i.d. × 6 cm) for data collection at 295 K over the 2θ range of 11 to 135° in steps of 0.05°. For these data collections, the detector array scanned the largest 2θ range allowable, i.e., ~40°, which has the effect of overlapping up to 15 detectors for steps in the middle of the pattern. Overlapping detectors for a given step serves to average the counting efficiency and the 2θ zero-point shift for each detector.

The least-squares structural refinements were made using the computer program GSAS (10), which employs a full-profile Rietveld analysis (11). Previous refinements of monoclinic ZrO_2 (IUCr Rietveld round-robin sample) showed a significantly improved fit using the pseudo-Voigt peak-profile function as described by Thompson *et al.* (12) as compared to the Voigt peak-profile function (11), without marked changes in the refined structural parameters, but with smaller standard errors. This implies that data from the HB-4 diffractometer is relatively high resolution, and the use of the pseudo-Voigt peak-profile function is appropriate. In the GSAS software, the pseudo-Voigt function is integrated using a multiterm Simpson's rule (13). A detailed description of the peak-profile function parameters and their interpretation is given by Larson and Von Dreele (10) and Von Dreele (14); the essential features are summarized here. The 2θ difference, ΔT, is modified for asymmetry, A_s, and sample shift, S_s, as $\Delta T' = \Delta T + f_i A_s/\tan 2\theta + S_s \cos\theta$. The width of the peak, σ^2, varies with 2θ as $\sigma^2 = U\tan^2\theta + V\tan\theta + W + P/\cos^2\theta$, where U, V, and W are the coefficients described by Caglioti *et al.* (15), and P is the Scherrer coefficient for Gaussian broadening. Preliminary refinements indicated that there was no Gaussian broadening so P was not refined. The Lorentzian coefficient, γ, varies as $\gamma = X/\cos\theta + Y\tan\theta + Z$, where the first term represents the Lorentzian Scherrer broadening, and the second term describes strain broadening. This function provides a better fit to asymmetric profiles and shows less correlation with the cell dimensions (10, 14). The peak-profiles were truncated at 0.3% of the peak height. The background was defined by a cosine Fourier series with 4 terms refined simultaneously with the other profile and structural parameters. The coherent scattering lengths were used: Sc (12.30), Y (7.75), Ce (4.84), Pr (4.45), Nd (7.69), Tb (7.38), Ho (8.08), Er (7.90), Tm (7.05), Yb (12.40), Lu (7.30), V (−0.38), and O (5.81) fm (16). Intensities were corrected for the Lorentz effect. No absorption correction was applied because it is indistinguishable from thermal motion effects. Low- and high-angle portions of the patterns for which only a single detector contributed were excluded which limited the data sets to the 2θ angular range of 13.75° to 132°, or to d-spacings of 5.846 to 0.7660 Å. No reflections occurred in the excluded region at low angles. The function minimized in the least-squares procedure was $\Sigma w_i(Y_{io} - Y_{ic})^2$, where Y_{io} and Y_{ic} are the observed and calculated intensities at each step i in the pattern. The weight w_i assigned to each step intensity is the reciprocal of the variance σ_i^2 at the ith step and was evaluated by $w_i = 1/\sigma_i^2 \approx n/Y_{io}$ where n is the number of detectors contributing to the average step intensity. The following agreement factors were calculated:

$$R_p = \sigma|Y_{io} - Y_{ic}|/\Sigma Y_{io}$$

$$R_{wp} = [\Sigma w_i(Y_{io} - Y_{ic})^2/\Sigma w_i Y_{io}^2]^{1/2}$$

$$R_{exp} = [(N - P)/\Sigma w_i Y_{io}^2]^{1/2}$$

$$\text{Goodness-of-fit} = \Sigma w_i(Y_{io} - Y_{ic})^2/(N - P),$$

TABLE 1
Crystal Data for Zircon-Type MVO_4 (M = Sc, Y, Ce, Pr, Nd, Tb, Ho, Er, Tm, Yb, Lu) Structure Refinements

	$ScVO_4$	YVO_4	$CeVO_4$	$PrVO_4$	$NdVO_4$	$TbVO_4$	$HoVO_4$	$ErVO_4$	$TmVO_4$	$YbVO_4$	$LuVO_4$
R_{wp}	0.0511	0.0452	0.0498	0.0441	0.0415	0.0382	0.0361	0.0405	0.0394	0.0405	0.0466
R_p	0.0421	0.0382	0.0415	0.0366	0.0352	0.0329	0.0313	0.0346	0.0341	0.0351	0.0396
R_{exp}	0.0375	0.0373	0.0356	0.0343	0.0333	0.0322	0.0316	0.0368	0.0356	0.0301	0.0402
G-of-F	1.853	1.462	1.962	1.654	1.545	1.406	1.300	1.210	1.222	1.705	1.339
a (Å)	6.7804 (1)	7.1183 (1)	7.4004 (2)	7.3631 (1)	7.3308 (1)	7.1774 (1)	7.1227 (1)	7.0957 (2)	7.0682 (1)	7.0427 (1)	7.0254 (1)
c (Å)	6.1345 (1)	6.2893 (1)	6.4972 (1)	6.4650 (1)	6.4356 (1)	6.3264 (1)	6.2891 (1)	6.2729 (1)	6.2593 (1)	6.2472 (1)	6.2347 (1)
$U_{eq}(M)^a$	0.54	0.40	0.41	0.39	0.25	0.24	0.15	0.19	0.16	0.27	0.35
y (O)	0.4428 (1)	0.4342 (1)	0.4279 (1)	0.4288 (1)	0.4295 (1)	0.4330 (1)	0.4341 (1)	0.4349 (1)	0.4355 (1)	0.4362 (1)	0.4364 (1)
z (O)	0.1967 (1)	0.2008 (1)	0.2067 (1)	0.2057 (1)	0.2050 (1)	0.2021 (1)	0.2010 (1)	0.2004 (1)	0.2001 (1)	0.2000 (1)	0.1995 (1)
$U_{eq}(O)^a$	0.50	0.73	0.97	0.94	0.91	0.80	0.81	0.53	0.62	0.70	0.65
V (Å^3)	282.03 (2)	318.68 (2)	355.83 (2)	350.51 (2)	345.85 (2)	325.90 (2)	319.06 (2)	315.84 (2)	312.71 (2)	309.85 (1)	307.72 (2)
M_r	159.89	203.84	255.06	255.84	259.18	273.86	279.87	282.20	283.87	287.98	289.61
D_x g/cm^3)	3.764	4.247	4.760	4.847	4.976	5.580	5.825	5.933	6.028	6.172	6.249
No. of Reflections	100	110	123	121	118	113	112	108	108	104	104
μR	0.405	0.059	0.048	0.142	0.436	0.463	0.703	1.706	1.237	0.419	1.155
Color	brown	tan	black	green	gray	brown	peach	pink	yellow	tan	beige

Note. Space group $I4_1/amd$, (No. 141, origin = 8c .2/m.). Atom positions are M on 4a; V on 4b, and O on 16h.
[a] Equivalent isotropic U_{eq} ($\times 10^3$Å^2) defined as one-third the trace of the orthogonalized U tensor.

TABLE 2
Selected Interatomic Distances (Å) and Angles (°) for Zircon-Type Compounds

	$ScVO_4$	YVO_4	$CeVO_4$	$PrVO_4$	$NdVO_4$	$TbVO_4$	$HoVO_4$	$ErVO_4$	$TmVO_4$	$YbVO_4$	$LuVO_4$
						VO_4 tetrahedra					
V–O ×4	1.7046 (9)	1.7088 (7)	1.7116 (8)	1.7120 (7)	1.7111 (7)	1.7091 (7)	1.7080 (8)	1.7090 (9)	1.7079 (7)	1.7077 (6)	1.7067 (7)
O...O ×4	2.864 (1)	2.870 (1)	2.872 (1)	2.873 (1)	2.871 (1)	2.869 (1)	2.868 (1)	2.870 (1)	2.868 (1)	2.867 (1)	2.866 (1)
O...O ×2	2.614 (1)	2.623 (1)	2.633 (1)	2.633 (1)	2.632 (1)	2.627 (1)	2.623 (1)	2.624 (1)	2.622 (1)	2.623 (1)	2.620 (1)
O–V–O ×4	114.31 (3)	114.25 (2)	114.08 (2)	114.10 (2)	114.10 (2)	114.16 (2)	114.22 (2)	114.22 (2)	114.23 (2)	114.18 (2)	114.24 (2)
O–V–O ×2	100.17 (6)	100.28 (4)	100.60 (5)	100.56 (4)	100.56 (5)	100.44 (4)	100.34 (5)	100.33 (5)	100.31 (4)	100.40 (4)	100.29 (4)
						MO_8 bisdisphenoids					
M–O ×4	2.3673 (9)	2.4333 (6)	2.5258 (7)	2.5114 (6)	2.4990 (7)	2.4513 (7)	2.4342 (7)	2.4272 (8)	2.4212 (7)	2.4175 (6)	2.4108 (7)
M–O ×4	2.1287 (8)	2.2975 (6)	2.4417 (8)	2.4217 (7)	2.4051 (7)	2.3269 (7)	2.2999 (7)	2.2851 (8)	2.2721 (7)	2.2586 (6)	2.2511 (6)
mean	2.2480	2.3654	2.4837	2.4665	2.4520	2.3891	2.3670	2.3561	2.3466	2.3380	2.3309
O...O ×2	2.614 (1)	2.623 (1)	2.633 (1)	2.633 (1)	2.632 (1)	2.627 (1)	2.623 (1)	2.624 (1)	2.622 (1)	2.623 (1)	2.620 (1)
O...O ×4	2.534 (1)	2.694 (1)	2.890 (1)	2.859 (1)	2.834 (1)	2.732 (1)	2.697 (1)	2.679 (1)	2.666 (1)	2.655 (1)	2.643 (1)
O...O ×8	2.8981 (2)	3.0403 (2)	3.1706 (3)	3.1525 (2)	3.1368 (2)	3.0664 (2)	3.0419 (2)	3.0297 (2)	3.0181 (2)	3.0069 (2)	2.9995 (2)
O...O ×4	3.074 (1)	3.318 (1)	3.533 (1)	3.503 (1)	3.478 (1)	3.362 (10)	3.322 (1)	3.300 (1)	3.281 (1)	3.262 (1)	3.250 (1)
O–*M*–O ×2	67.05 (4)	65.23 (3)	62.85 (4)	63.24 (3)	63.56 (3)	64.80 (3)	65.21 (4)	65.46 (4)	65.58 (3)	65.73 (3)	65.84 (3)
O–*M*–O ×4	68.40 (4)	69.36 (2)	71.13 (2)	70.82 (2)	70.59 (2)	69.70 (2)	69.39 (3)	69.23 (4)	69.16 (2)	69.10 (2)	69.00 (2)
O–*M*–O ×8	80.08 (2)	79.92 (1)	79.30 (1)	79.42 (1)	79.50 (1)	79.80 (1)	79.91 (1)	79.96 (1)	79.97 (1)	79.96 (1)	80.01 (1)
O–*M*–O ×4	92.44 (1)	92.472 (7)	92.710 (7)	92.665 (7)	92.632 (7)	92.521 (7)	92.478 (8)	92.461 (9)	92.458 (7)	92.468 (7)	92.446 (7)

where N and P are the number of observations and adjustable parameters, respectively.

Starting values for the structural parameters for the refinements were obtained from the structure data of zircon (17), and starting values for the peak-profile function parameters were assigned based on a previous refinement of monoclinic ZrO_2. Vanadium does not significantly contribute to the structure-factor expression because it has a near-zero scattering length, therefore a meaningful displacement parameter for the V atom could not be refined and was fixed at 0.005 Å.[2] A model with anisotropic displacement parameters for the oxygen and M atoms was significantly better (at the 1% significance level) than an isotropic model in each case, as determined using the R-factor ratio test (18). In all, 22 parameters (18 for the isotropic model) were refined, and the least-squares refinements were continued until the sum of the squared errors, i.e., (parameter shifts/esd),[2] was less than 1%. The largest element in each of the correlation matrices between the structural parameters was less than 0.5.

STRUCTURE DESCRIPTIONS

Conceptually, the MVO_4 zircon-type structure is built from chains of alternating edge-sharing VO_4 tetrahedra and MO_8 bisdisphenoids extending parallel to c and joined laterally by edge-sharing bisdisphenoids, which themselves form "zigzag" chains parallel to a. The zircon structure has space group symmetry $I4_1/amd$, $Z = 4$, and 3 atoms occupy the asymmetric unit. A summary of the refined structural parameters, agreement indices, final positional parameters, and equivalent isotropic displacement parameters are given in Table 1. Selected bond lengths and angles are given in Table 2. The refined anisotropic displacement parameters are given in Table 3.[1] Nonpositive definite temperature factors occurred for 3 atoms out of 22, which is not surprising because the d-spacing range of the data only extended down to 0.766 Å. Examples of the corresponding observed, calculated, and difference neutron powder diffraction profiles are presented in Fig. 1.[1] The VO_4 tetrahedron is slightly elongated because the O...O edges shared with the bisdisphenoids are about 8% shorter than those polyhedral edges not shared (Table 2). The MO_8 bisdisphenoid has two sets of M–O bond distances, four long bonds to the edges shared with tetrahedra and four shorter bonds to the edges shared with other bisdisphenoids. The bisdisphenoid coordination polyhedron can be viewed as two interpenetrating tetrahedra, one elongated and the other compressed, and both having a common $\bar{4}$ axis. Except for $ScVO_4$, MO_8 bisdisphenoids of the other zircon vanadates have the shortest O...O distance shared between the tetrahedron and the bisdisphenoid, and the next shortest shared between two bisdisphenoids. The unshared edges of the bisdisphenoids are divided into two sets. For $ScVO_4$, the shared O...O edge between bisdisphenoids is smaller than that shared between the tetrahedron and bisdisphenoid because of the small size of the Sc ion. Nyman *et al.* (19), have described the common occurrence of the bisdisphenoid-coordination polyhedra in a number of important ABX_4 crystal structures (e.g., zircon, anhydrite, scheelite)

[1] The list of step-scan diffraction data and refined anisotropic displacement parameters has been deposited with the British Library Document Supply Centre as Supplementary Publication No. 99999 (23 pp.). Copies may be obtained through the Technical Editor, International Union of Crystallography, 5 Abbey Square, Chester CH1 2HU, England.

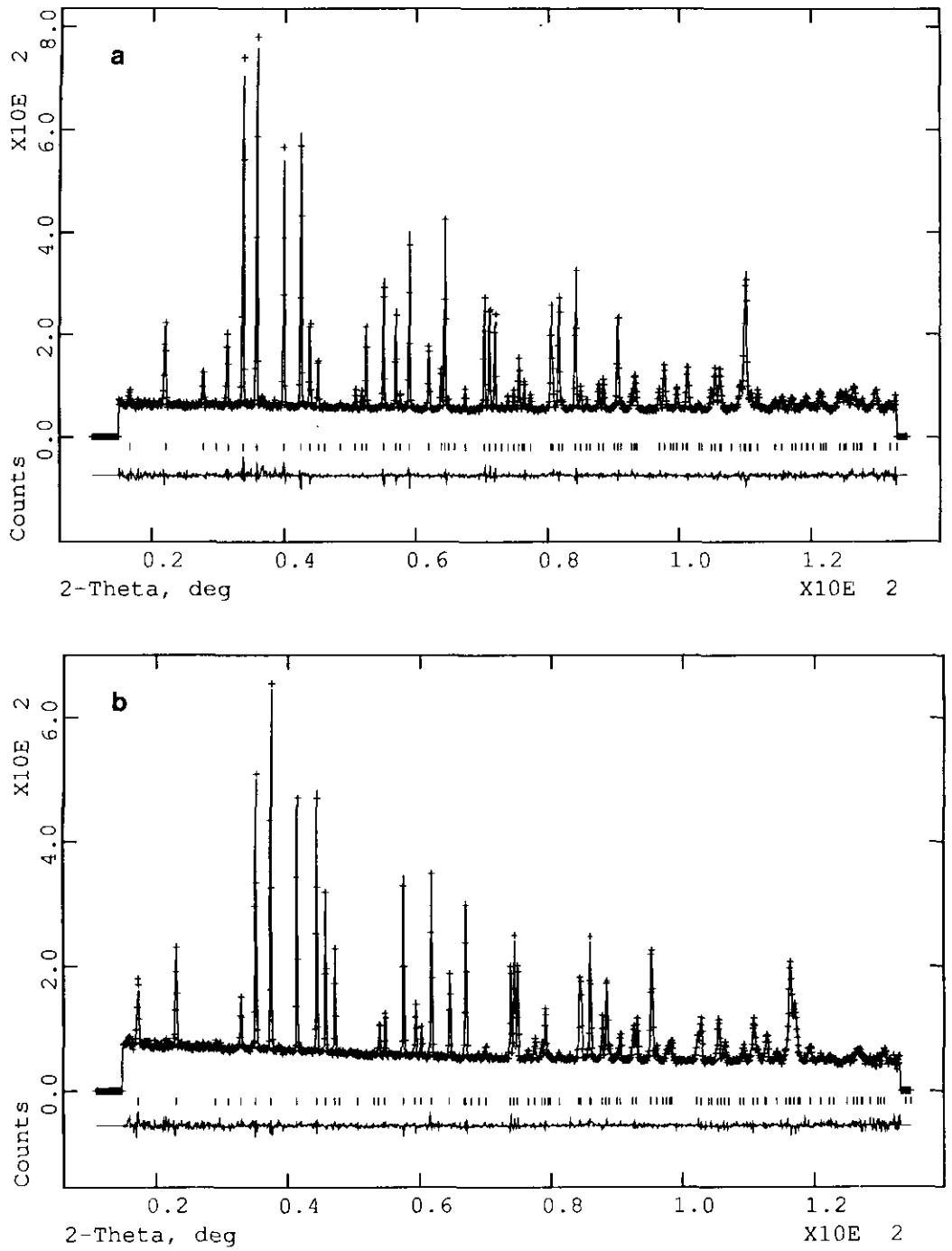

FIG. 1. Representative observed, calculated, and difference neutron powder-diffraction profiles for MVO_4: (a) M = Pr, (b) M = Tm, and (c) M = Lu. The observed data are indicated by crosses, and the calculated profile is the continuous solid line in the same field. The short vertical lines below the profiles mark the positions of all possible Bragg reflections, and the bottom curve is the difference between the observed and calculated intensity (plotted using the same vertical scale as the observed and calculated profiles).

and have illustrated the simple structural relationships via crystallographic twin operations.

The variation of the oxygen position as a function of atomic number for the $LnVO_4$ samples determined in this study has been compared with previously reported values taken from the literature (see Fig. 2). The oxygen displacement about its mean position is highly anisotropic with the maximum vibration amplitude perpendicular to the edge shared between the VO_4 tetrahedron and the MO_8 bisdisphenoid.

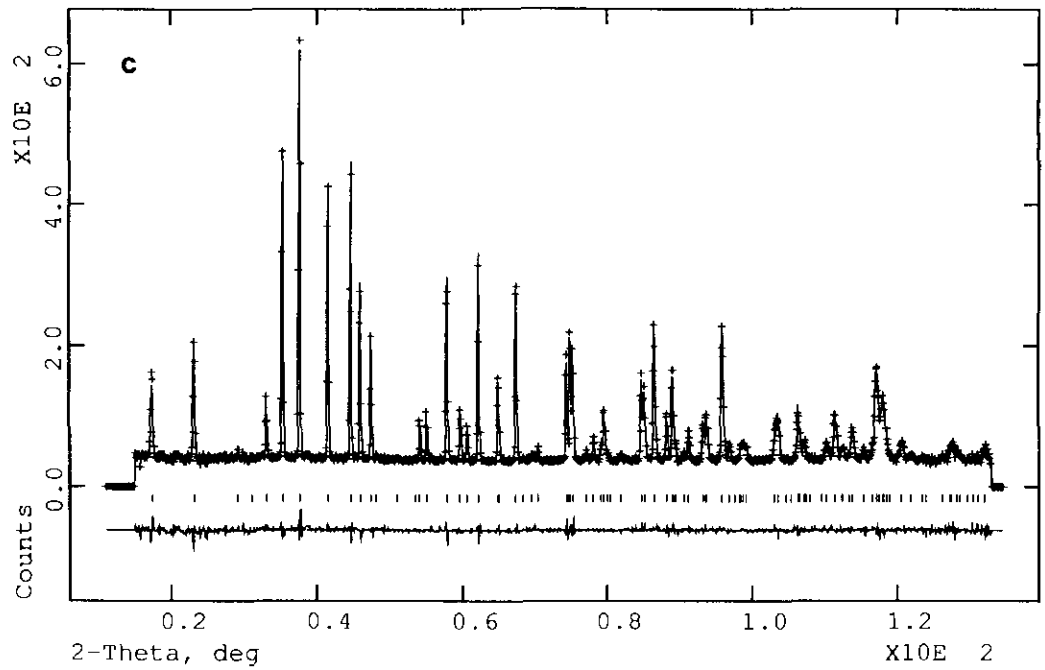

FIG. 1—*Continued*

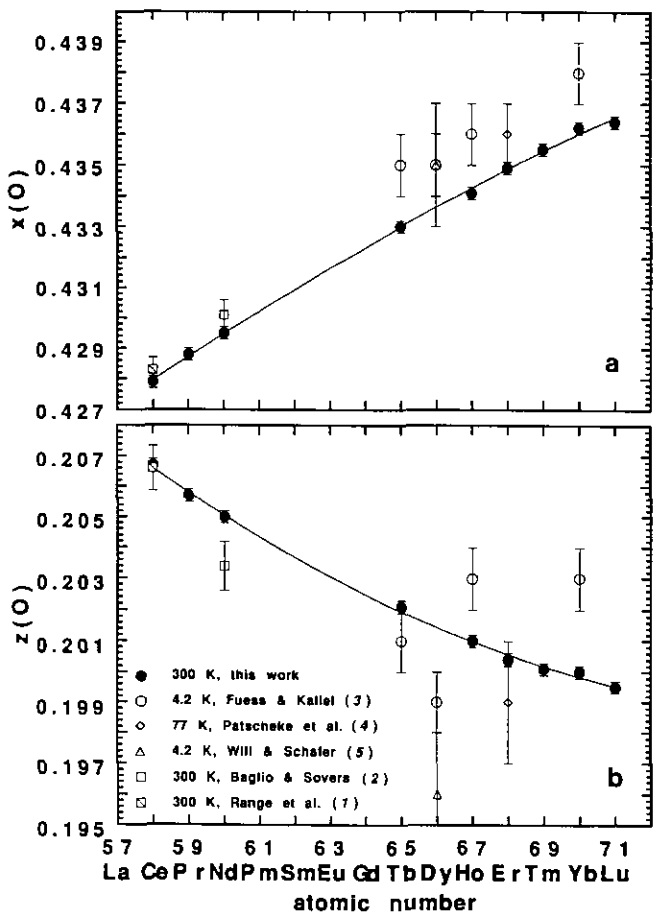

FIG. 2. Variation of the oxygen-atom positional parameters for $LnVO_4$ as a function of atomic number: (a) oxygen x positional parameter, (b) oxygen z positional parameter. The legend defines symbols used in both plots for values taken from the literature and also gives the temperatures at which the diffraction data were collected. The error bars show +/− one estimated standard error for values taken from the literature and +/− two estimated standard errors for values determined in this study.

TABLE 3

Anisotropic Displacement Parameters[a] (×10³ Å²) for Zircon-Type MVO_4 (M = Sc, Y, Ce, Pr, Nd, Tb, Ho, Er, Tm, Yb, Lu)[b]

	U_{11}	U_{22}	U_{33}	U_{12}	U_{13}	U_{23}
Sc	5.2 (4)	5.2 (4)	5.9 (5)	0	0	0
O[c]	9.0 (5)	0.7 (5)	5.3 (6)	0	0	2.4 (3)
Y	4.1 (3)	4.1 (3)	3.7 (4)	0	0	0
O	13.1 (3)	4.1 (3)	4.7 (3)	0	0	1.4 (3)
Ce[c]	7.8 (6)	7.8 (6)	−3.1 (7)	0	0	0
O	19.4 (5)	7.9 (4)	1.5 (3)	0	0	0.7 (3)
Pr	5.6 (5)	5.6 (5)	0.6 (7)	0	0	0
O	17.3 (4)	6.5 (3)	4.4 (2)	0	0	0.9 (3)
Nd[c]	3.7 (3)	3.7 (3)	−0.1 (5)	0	0	0
O	15.6 (4)	5.9 (4)	5.6 (3)	0	0	0.6 (3)
Tb	3.1 (3)	3.1 (3)	1.0 (5)	0	0	0
O	14.4 (4)	3.6 (3)	5.9 (3)	0	0	1.0 (3)
Ho	2.0 (3)	2.0 (3)	0.3 (5)	0	0	0
O	13.8 (4)	4.9 (4)	5.4 (4)	0	0	1.0 (3)
Er	2.6 (4)	2.6 (4)	0.3 (6)	0	0	0
O	10.7 (5)	2.4 (4)	2.6 (4)	0	0	0.7 (4)
Tm	2.1 (3)	2.1 (3)	0.6 (5)	0	0	0
O	12.1 (4)	2.9 (3)	3.6 (3)	0	0	1.4 (3)
Yb	3.0 (2)	3.0 (2)	1.9 (3)	0	0	0
O	12.5 (3)	3.6 (4)	4.7 (3)	0	0	1.6 (3)
Lu	4.2 (3)	4.1 (3)	2.0 (5)	0	0	0
O	11.5 (4)	3.4 (4)	4.5 (3)	0	0	1.6 (3)

[a] The temperature factor expression has the form $\exp[-2\pi^2(U_{11}h^2a^{*2} + U_{22}k^2b^{*2} + U_{33}l^2c^{*2} + 2U_{12}hka^*b^* \cos\gamma^* + 2U_{13}hla^*c^* \cos\beta^* + 2U_{23}klb^*c^* \cos\alpha^*)]$ where U_{ij} are the mean-square amplitudes of vibration.

[b] The temperature factor for V was fixed at 0.005 Å².

[c] Ellipsoid is nonpositive definite.

TABLE 4

Empirical Relationships between Crystal Structure Parameters of Zircon-Type $LnVO_4$ and Lanthanide Ionic Radii (R)[a]

Cell dimensions	
$a = (2.6809 + 6.3244R - 1.9221R^2)$ Å	$r^2 = 0.999$
$c = (6.2173 - 1.3048R + 1.3548R^2)$ Å	$r^2 = 0.999$
Oxygen positional parameters[b]	
$x = 0.4864 - 0.05126R$	$r^2 = 0.997$
$z = 0.1577 + 0.04269R$	$r^2 = 0.997$

[a] Ionic radii from Shannon (20).
[b] Space group $I4_1/amd$ (No. 141, origin, 8c .2/m).

DISCUSSION

Given the high precision of the present structural refinements for the zircon-type $LnVO_4$ series, empirical relationships between the structural parameters and lanthanide ionic radii from Shannon (20) have been determined by the method of least-squares (Table 4). These equations permit the estimation of structural parameters for vanadate solid solutions and other lanthanide end-member zircon-type vanadates not refined in this study. Note that the variation of the oxygen positional parameters x and z has been calculated previously for the zircon-type lanthanide vanadates by Baglio and Sovers (2). These workers used a semiempirical approach, employing results of their own refinement of $NdVO_4$ and that of $ErVO_4$ (4) to constrain the cell dimensions and space group, in order to minimize the lattice energy as a function of the oxygen position. However, of the several models with various structural constraints that they present, none correctly computed the observed variation of the oxygen position for the lanthanide series.

The oxygen displacement about its mean position is highly anisotropic in the zircon-type vanadates. This is, however, generally not the case for the zircon-type $LnPO_4$ compounds whose structures have been refined previously (21–24). This difference probably reflects the more compact and rigid nature of the PO_4 tetrahedron as compared to the VO_4 tetrahedron.

ACKNOWLEDGMENTS

We thank Jaime Fernandez-Baca for assistance in running the HB4 diffractometer. This research was supported by the Division of Materials Sciences, U.S. Department of Energy under Contract DE-AC05-84OR21400 with Martin Marietta Energy Systems.

REFERENCES

1. K-J. Range, H. Meister, and U. Klement, *Z. Naturforsch. B* **45,** 598 (1990).
2. J. A. Baglio and O. J. Sovers, *J. Solid State Chem.* **3,** 458 (1971).
3. H. Fuess and A. Kallel, *J. Solid State Chem.* **5,** 11 (1972).
4. E. Patscheke, H. Fuess, and G. Will, *Chem. Phys. Lett.* **2,** 47 (1968).
5. G. Will and W. Schafer, *J. Phys. C Solid State Phys.* **4,** 811 (1971).
6. M. M. Abraham, L. A. Boatner, T. C. Quinby, D. K. Thomas, and M. Rappaz, *Radioact. Waste Manage.* **1,** 181 (1980).
7. L. A. Boatner and B. C. Sales, "Radioactive Waste Forms for the Future" (W. Lutze and R. C. Ewing, Ed.), p. 507. Elsevier, New York, 1988.
8. R. C. Ropp and B. Carroll, *J. Inorg. Nucl. Chem.* **35,** 1153 (1973).
9. Von M. E. Escobar and E. J. Baran, *Z. Anorg. Allg. Chem.* **441,** 273 (1978).
10. A. C. Larson and R. B. Von Dreele, "GSAS—General Structure Analysis System," Report LA-UR-86-748, Los Alamos National Laboratory, Los Alamos, NM, 1990.
11. H. M. Rietveld, *J. Appl. Crystallogr.* **2,** 65 (1969).
12. P. Thompson, D. E. Cox, and J. B. Hastings, *J. Appl. Crystallogr.* **20,** 79 (1987).
13. C. J. Howard, *J. Appl. Crystallogr.* **15,** 615 (1982).
14. R. B. Von Dreele, "Modern Powder Diffraction" (D. L. Bish and J. E. Post, Ed.), p. 333. Mineral. Soc. Am., Washington, DC, 1989.
15. G. Caglioti, A. Paoletti, and F. P. Ricci, *Nucl. Instrum.* **3,** 223 (1958).
16. V. F. Sears, "Methods of Experimental Physics" (K. Skold and D. L. Price, Ed.), Vol. 23, Part A, p. 521, Academic Press, Orlando, 1986.
17. R. M. Hazen and L. W. Finger, *Am. Mineral.* **64,** 196 (1979).
18. W. C. Hamilton, "International Tables for X-ray Crystallography" (J. A. Ibers and W. C. Hamilton, Ed.), Vol. 4, p. 288. Kynoch Press, Birmingham, 1974.
19. H. Nyman, B. G. Hyde, and S. Andersson, *Acta Crystallogr. Sect. B* **40,** 441 (1984).
20. R. D. Shannon, *Acta Crystallogr. Sect. A* **32,** 751 (1976).
21. W. O. Milligan, D. F. Mullica, G. W. Beall, and L. A. Boatner, *Inorg. Chem. Acta* **60,** 39 (1982).
22. W. O. Milligan, D. F. Mullica, G. W. Beall, and L. A. Boatner, *Inorg. Chem. Acta* **70,** 133 (1983).
23. W. O. Milligan, D. F. Mullica, G. W. Beall, and L. A. Boatner, *Acta Crystallogr. Sect. C* **39,** 23 (1983).
24. D. F. Mullica, E. L. Sappenfield, and L. A. Boatner, *Inorg. Chem. Acta* **174,** 155 (1990).